Computers & Geosciences 36 (2010) 167–170

Contents lists available at ScienceDirect

Computers & Geosciences

journal homepage: www.elsevier.com/locate/cageo

Spatio-spectral heterogeneity analysis using EO-1 Hyperion imagery

Weirong Chen *, Geoffrey M. Henebry [1]

Center for Advanced Land Management Information Technologies (CALMIT), School of Natural Resources, University of Nebraska-Lincoln, Lincoln, NE 68583-0961, USA

ARTICLE INFO

Article history:
Received 1 June 2008
Received in revised form
12 April 2009
Accepted 18 May 2009

Keywords:
Hyperspectral imagery
Semivariogram analysis
Spatio-spectral heterogeneity

ABSTRACT

How does observed spatial structure change as a function of spectral wavelength and resolution? The fine spectral resolution data of a Hyperion image acquired over agricultural research fields in eastern Nebraska, USA, were analyzed using variography to characterize spatial patterns within each wavelength-specific image. The geospatial analysis was repeated simulating Landsat TM/ETM+ bands from the Hyperion data. Significant changes in spatio-spectral heterogeneity were observed across the red edge. The total amount of spatial variability is closely correlated to the contrast in brightness of objects within the scene. The spatial dependence in an image is also influenced by differential brightness, but to a lesser extent. Increasing bandwidth may blur spatial structure that occurs at finer spectral resolution, resulting in the loss of spatial structure that may relate to significant features within the scene.

1. Introduction

Spectral reflectance from surface features can vary by wavelength. The magnitude of this variation can change from one region of the electromagnetic spectrum to another. Hence, the spatial arrangement of brightness values within an image – the texture – is affected by the specific wavelengths sampled. With the technical successes of the Hyperion imaging spectrometer aboard NASA's EO-1 satellite and the prospect of the Decadal Survey mission HyspIRI – there is an unprecedented opportunity to use the fine spectral resolution data to examine the differences in spatial pattern across dozens of bands. Such research will improve our understanding of spatio-spectral heterogeneity, i.e., how observed spatial patterns change as a function of spectral wavelengths (Goodin and Henebry, 1998; Goodin et al., 2004; Garrigues et al., 2006). Such information can be used to design optimal sampling schemes across wavelengths (Atkinson and Emery, 1999).

Most previous research in this area has concentrated on characterizing spatial structure using the broadband spectra. Briggs and Nellis (1991) measured the seasonal variation of spatial heterogeneity in tallgrass prairie by using a simple textural measure applied to seven different SPOT scenes acquired across a growing season. They found more spatial heterogeneity, in terms of contrast, in the near infrared (NIR) than in the visible bands, as well as seasonal variation in the spatial pattern. Analyzing six Landsat TM and SPOT scenes acquired over different regions, Chavez (1992) also found that the spatial variability from place to place is greater in the NIR band than in the visible band, especially in images covering densely vegetated areas. Using a non-imaging spectrometer that emulated Landsat TM bands with hierarchical spatial sampling in tallgrass prairie, Goodin and Henebry (1998) demonstrated differences in the spatial dependence of NDVI and its component bands during the growing season and as a function of treatment by prescribed burning. Atkinson and Emery (1999) collected reflectance spectra in 252 wavebands in the visible and NIR at close range. They found that while both the amount and variation of spatial variability were much greater in the NIR wavelengths than in the visible wavelengths for their two study sites; spatial dependence showed mixed results. Although hyperspectral data were employed in their study, spatial structure was examined by integrating bands across the visible or NIR region, rather than a band-by-band analysis. Further, no investigation was made in terms of the effect of spectral resolution on spatial structure, which is necessary to understand the difference between broadband and narrowband spectra in characterizing spatial pattern. Here we apply semivariogram analysis to investigate spatio-spectral heterogeneity in a hyperspectral image of a diverse agricultural landscape.

2. Methods

2.1. Study area, Hyperion imagery acquisition and preprocessing

The study area is the University of Nebraska's Agricultural Research and Development Center (ARDC), a 3846 ha of farmland

* Corresponding author. Present address: Canada Centre for Remote Sensing, 588 Booth Street, Ottawa, Ontario, Canada K1A 0Y7. Tel.: +1 613 947 1254; fax: +1 613 947 1385.
E-mail addresses: weirong.chen@nrcan.gc.ca, weirong.chen@yahoo.com (W. Chen).
[1] G.M. Henebry is now with the Geographic Information Science Center of Excellence (GIScCE), South Dakota State University, Brookings, SD 57007-3510, USA.

0098-3004/$ - see front matter © 2009 Elsevier Ltd. All rights reserved.
doi:10.1016/j.cageo.2009.05.005

located 48 km north of Lincoln near Mead, Nebraska, USA (41°8′N, 96°30′W) (Fig. 1). ARDC is a major research and educational facility in the Agricultural Research Division of the University of Nebraska's Institute of Agriculture and Natural Resources and serves as the primary site for field research.

Hyperion acquired the image used in the study on August 29, 2001. One of three sensors aboard EO-1, Hyperion has 242 bands within the 0.4–2.5 μm spectral region; each band is about 10 nm wide. Two detector arrays cover this wavelength range, one for the visible and near infrared (VNIR: 356–1058 nm) and the other for the short-wave infrared (SWIR: 852–2577 nm) (Staenz et al., 2002). The swath width is a relatively narrow at 7.5 km, but the spatial resolution, at 30 m, resembles the visible, NIR, and shortwave-infrared (SWIR) bands on the Landsat TM and ETM+ sensors.

We focused our analysis on a subset of these 242 bands to avoid the poor signal-to-noise ration resulting from the strong atmospheric absorption at some wavelengths and to minimize the striping artifacts induced by inaccurate radiometric calibration across the detector array. We selected three broad regions for analysis: bands 12–55 (468–906 nm), bands 134–163 (1488–1780 nm), and bands 188–218 (2032–2335 nm), which correspond to Landsat TM/ETM+ bands 1–4, 5, and 7, respectively. The spectrally subset image was georeferenced to a USGS 1:12,000 digital orthophoto quadrangle (DOQ). To reduce the atmospheric influence in the data and to compensate the decrease in solar irradiance at longer wavelengths, we radiometrically normalized the image bands using a flat-field correction. First, we subtracted the bias, which was determined through evaluating a histogram of brightness values of a reference target (clear deep water) found in all bands (Jensen, 1996). Second, we divided each pixel's spectrum by the mean value of a spectrally uniform, highly reflective area (i.e., a parking lot) found in the scene (Rast et al., 1991; Schowengerdt, 1997). Finally, the result was further rescaled to a byte representation to facilitate the spatial analyses. While Hyperion exhibits a "spectral smile" resulting in systematic non-uniform response across the detector arrays (Liao et al., 2000), this low spatial frequency bias was not a significant contributor to the high spatial frequency structure characterized here.

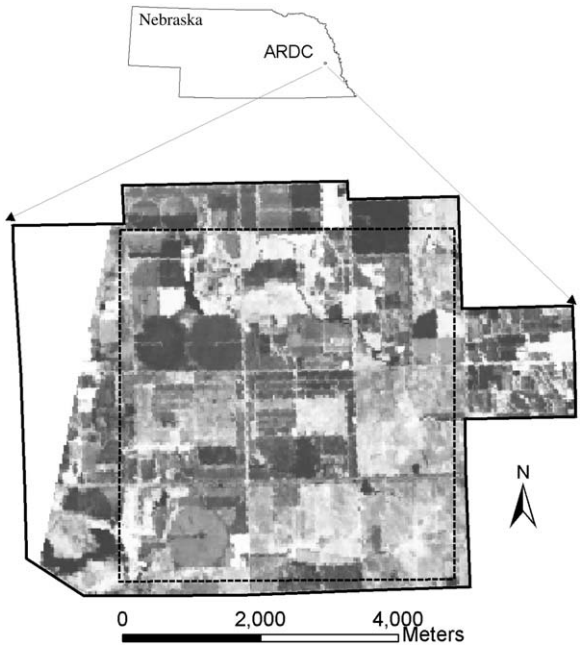

Fig. 1. Location and extent of ARDC and an image that is sum of all bands selected for study. Dashed rectangle indicates area covered by data actually used in study.

2.2. Semivariogram analysis

Semivariance $\gamma(h)$ is half the expected squared difference between pairs of pixels at a distance of separation or lag, h, a vector in both distance and direction. A semivariogram displays the relationship between semivariance and the (directed) distance separating samples. The shape of a stationary semivariogram can frequently be summarized using the spherical model (Cohen et al., 1990). The parameter coefficients of the spherical model provide a concise means to characterize the data's spatial structure; specifically, here we use the range (a_o) and the sill plus nugget variance ($c+c_o$). This latter sum corresponds to the dataset's total amount of spatial variability or maximum level of $\gamma(h)$. The lag distance at which this maximum is reached is the range (a_o) of the semivariogram, indicating the extent of the spatial dependence in the data. Pairs of pixels separated by more than this lag distance are presumed to be statistically independent (Curran, 1988).

Given the irregular shape of the ARDC and the lack of data over part of the area, we restricted semivariance calculations to a square subset corresponding to 2464 ha (Fig. 1). Semivariance was calculated along each row (west–east orientation) and column (north–south orientation) using the GSLIB 2.0 software (Deutsch and Journel, 1998). The final semivariogram of each direction used in the analysis was the average of the semivariograms obtained for that direction. To observe the effect of spectral resolution on the characterization of spatial structure, we rescaled the Hyperion bands by simple averaging to simulate the broader Landsat bands. Semivariance was then calculated for each simulated band. Fitting a spherical model to each band's semivariogram, the parameters $c+c_o$ and a_o were identified interactively using VARIOWIN software (Pannatier, 1996). The "indicative goodness of fit" (IGF) statistic provided by VARIOWIN characterized model fit by this unitless, standardized measure (Pannatier, 1996). Our IGF values ranged for all models from 0.0037 to 0.0246, indicating very good agreement of the models with the data (Levesque and King, 1999).

3. Results and discussion

The Hyperion scene displays strong spatio-spectral heterogeneity. In both the north–south and west–east directions, there are dramatic changes in the total amount of spatial variability, as measured by $c+c_o$, across the transition from visible to NIR wavelengths (Fig. 2A). The much higher variability observed in the NIR agrees with Briggs and Nellis (1991), Chavez (1992), Goodin and Henebry (1998) and Atkinson and Emery (1999), but the finer spectral resolution of Hyperion reveals significant details about the red edge transition. While $c+c_o$ decreases in the SWIR wavelengths, it remains higher than in the visible (Fig. 2B). A local maximum of $c+c_o$ at 2204 nm is bounded by local minima occurring at 2174 and at 2274 nm. Some directional differentiation in the $c+c_o$ is evident: from about 8.5% across the visible to less than 5% over the NIR and SWIR wavelengths.

Values of a_o as a function of wavelength exhibit substantial anisotropy, especially within the visible (Fig. 3A). As with $c+c_o$, there is a striking shift in a_o across the red edge. A linear increasing trend in a_o is apparent from a local minimum near 550–560 nm to the beginning of the red edge. A local trough at 712 nm is followed by a steep rise to a plateau beyond 743 nm. The response across the SWIR is nearly flat; the principal exception being a peak from 2174 to 2214 nm (Fig. 3B).

Total amount of spatial variability and spatial dependence in a particular band are related to the difference in reflectance of the scene object: the patterns of both $c+c_o$ and a_o closely track the pattern of the absolute difference in reflectance between soil and